ORIGINAL RESEARCH

DosS Is Required for the Complete Virulence of *Mycobacterium tuberculosis* in Mice with Classical Granulomatous Lesions

Uma S. Gautam[1], Amanda McGillivray[1], Smriti Mehra[2], Peter J. Didier[3], Cecily C. Midkiff[3], Ryan S. Kissee[1], Nadia A. Golden[1], Xavier Alvarez[3], Tianhua Niu[4], Jyothi Rengarajan[6], David R. Sherman[7], and Deepak Kaushal[1,5]

Divisions of [1]Bacteriology and Parasitology, [2]Microbiology, and [3]Comparative Pathology, Tulane National Primate Research Center, Covington, Louisiana; Departments of [4]Biostatistics & Bioinformatics and [5]Microbiology & Immunology, Tulane University School of Public Health and Tropical Medicine, New Orleans, Louisiana; [6]Yerkes National Primate Research Center, Atlanta, Georgia; and [7]Seattle Biomedical Research Institute, Seattle, Washington

Abstract

Mycobacterium tuberculosis (*Mtb*) must counter hypoxia within granulomas to persist. DosR, in concert with sensor kinases DosS and DosT, regulates the response to hypoxia. Yet *Mtb* lacking functional DosR colonize the lungs of C57Bl/6 mice, presumably owing to the lack of organized lesions with sufficient hypoxia in that model. We compared the phenotype of the Δ-*dos*R, Δ-*dos*S, and Δ-*dos*T mutants to *Mtb* using C3HeB/FeJ mice, an alternate mouse model where lesions develop hypoxia. C3HeB/FeJ mice were infected via aerosol. The progression of infection was analyzed by tissue bacterial burden and histopathology. A measure of the comparative global immune responses was also analyzed. Although Δ-*dos*R and Δ-*dos*T grew comparably to wild-type *Mtb*, Δ-*dos*S exhibited a significant defect in bacterial burden and pathology *in vivo*, accompanied by ablated proinflammatory response. Δ-*dos*S retained the ability to induce DosR. The Δ-*dos*S mutant was also attenuated in murine macrophages *ex vivo*, with evidence of reduced expression of the proinflammatory signature. Our results show that DosS, but not DosR and DosT, is required by *Mtb* to survive in C3HeB/FeJ mice. The attenuation of Δ-*dos*S is not due to its inability to induce the DosR regulon, nor is it a result of the accumulation of hypoxia. That the *in vivo* growth restriction of Δ-*dos*S could be mimicked *ex vivo* suggested sensitivity to macrophage oxidative burst. Anoxic caseous centers within tuberculosis lesions eventually progress to cavities. Our results provide greater insight into the molecular mechanisms of *Mtb* persistence within host lungs.

Keywords: *Mycobacterium tuberculosis*; hypoxia; response regulator; sensor kinase; latency

Clinical Relevance

Our research indicates that the C3HeB/FeJ mouse model is appropriate for the study of *Mycobacterium tuberculosis* pathogenesis because it reveals attenuation in the Δ-dosS mutation. It appears that this attenuation is not the result of hypoxia in lung granulomas.

A hallmark of human tuberculosis (TB) infection is the development of granulomatous lesions with central caseous necrosis (1). Granuloma formation attempts to contain the pathogen and may facilitate the survival and persistence in a state of reduced replication (2). It is within the granuloma that *Mtb* encounters hypoxia and responds via the induction of the DosR regulon (3). It has been postulated that this regulon is essential for bacterial survival and adaptation during

(Received in original form June 11, 2014; accepted in final form October 13, 2014)

This work was supported by National Institutes of Health grants AI089323, HL106790, AI091457, RR026006, RR020159, RR000164/OD011104, and C06AI058609, and by awards from Howard Hughes Medical Institutions, the Office of the Director, Tulane National Primate Research Center, the Tulane National Primate Research Center Pilot Projects Program, Louisiana Vaccine Center, Tulane Research Enhancement Fund, Tulane Center for Infectious Diseases, and a Bridge Fund from the Tulane Office of Vice-President for Research.

Author Contributions: Conception and design: U.S.G. and D.K. Acquisition of data: U.S.G., A.M., R.S.K., N.A.G., and D.K. Analysis and interpretation: U.S.G., S.M., T.N., J.R., P.J.D., D.R.S., D.K. Drafting the manuscript for important intellectual content: D.K. and U.S.G. with help from J.R., P.J.D., and D.R.S. Funding: D.K. Experimental research: C.C.M. and X.A.

Correspondence and requests for reprints should be addressed to Deepak Kaushal, Ph.D., Tulane National Primate Research Center, 18703 Three Rivers Road, Covington, LA 70433. E-mail: dkaushal@tulane.edu

This article has an online supplement, which is accessible from this issue's table of contents at www.atsjournals.org.

Am J Respir Cell Mol Biol Vol 52, Iss 6, pp 708–716, Jun 2015

Originally Published in Press as DOI: 10.1165/rcmb.2014-0230OC on October 16, 2014
Internet address: www.atsjournals.org

intragranulomatous persistence (4, 5), although the data linking DosR to survival or virulence in animals are equivocal (6–9).

Experimental *Mtb* infection in the traditional mouse model does not result in the formation of human-like centrally necrotic lung lesions (10), likely explaining the absence of reduced bacterial burdens phenotype in C57Bl/6 mice infected with the *Mtb*:Δ-*dos*R mutant (6). C57Bl/6 mice do not faithfully reproduce certain aspects of human TB. In contrast, *Mtb*-infected C3HeB/FeJ mice display lesions with prominent necrotic degeneration, thus more closely resembling human granulomas (11–15). Harper and colleagues first demonstrated that tubercle lesions in this model develop hypoxia (15). Hence, we investigated the effect of different mutations in the DosR regulon in C3HeB/FeJ mice by comparing the infection phenotypes of mice infected with low doses of mutants in response regulator DosR (Δ-*dos*R) or sensor kinases DosS (Δ-*dos*S) and DosT (Δ-*dos*T) relative to the parental *Mtb* strain. Δ-*dos*S, but none of the other mutants, exhibited reduced levels of bacterial burden, pulmonary pathology, and inflammation *in vivo* during early infection. However, infection with Δ-*dos*S did not result in different pathological manifestations. Δ-*dos*S retained the ability to induce the expression of the DosR regulon and exhibited reduced intraphagosomal growth, indicating a hypoxia-independent mechanism of its attenuation.

Materials and Methods

Mice and Infection

Mtb H37Rv and the various mutants were cultured as previously described (6, 16). Four groups of 28 male C3HeB/FeJ mice (5–6 wk old) (Jackson Laboratory, Bar Harbor, ME) were infected with approximately 100 CFUs of bacilli via aerosol (17) (Table 1). Initial bacterial deposition was determined by killing four mice from each group at Day 1 (17). Four mice per group were then killed every 4 weeks for CFU count, histopathology, and host immune response assays (Weeks 0, 4, 8, 12, 16, and 20).

The Tulane National Primate Research Center (TNPRC) facilities are accredited by the American Association for Accreditation of Laboratory Animal Care and licensed by the U.S. Department of Agriculture. All animals were routinely cared for according to the guidelines prescribed by the National Institutes of Health Guide to Laboratory Animal Care. Humane endpoints were predefined in this protocol and applied as a measure of reduction of discomfort. All procedures were approved by the Institutional Animal Care and Use Committee and the Institutional Biosafety Committee (IACUC). The TNPRC facilities are accredited by the American Association for Accreditation of Laboratory Animal Care (AAALAC) and licensed by the U.S. Department of Agriculture. The animal research program at the TNPRC is subject to oversight by IACUC. The animals are usually group-housed in appropriate social settings in accordance with the guidelines of AAALAC, which annually inspects all facilities. The IACUC performs semiannual and annual inspections of the facility to certify compliance with the highest possible levels of housing conditions, feeding regimens, and environmental enrichment. Specific steps were taken to provide physical care and to perform examinations in accordance with institutional endpoint policies. Experiments involving *Mtb* were approved by the Tulane Institutional Biosafety Committee.

Table 1. Pulmonary Bacterial Burdens in C3HeB/FeJ Mice after Aerosol Infection

Time Point, Day 1	Mean ± SD, $\log_{10}$ CFUs*
Mtb	1.75 ± 0.26
Mtb:Δ-*dos*R	1.87 ± 0.21
Mtb:Δ-*dos*S	1.98 ± 0.14
Mtb:Δ-*dos*T	1.86 ± 0.12

*Data are representative of multiple infections; four mice were used for each infection and time point. *Mtb*, *Mycobacterium tuberculosis*.

Staining Procedures, Histopathology, and Microscopy

Lung tissue was fixed for hematoxylin-eosin histology and confocal microscopy (18–22). Ten images of each slide were used for analysis (Inform; PerkinElmer, Waltham, MA). For pimonidazole (PIMO) immunohistochemistry, mice were intraperitoneally injected at each time point with 100 mg/kg body weight of PIMO (Hypoxyprobe, Burlington, MA) 90 minutes before being killed (23). Tissues were stained as described for PIMO (24) and Oil Red O (24, 25).

Transcript Measurements from Mycobacteria

To demonstrate a high level of hypoxia, *Mtb* wild-type mice and mutants were cultured as described with minor modifications (6, 26). Briefly, frozen stocks of *Mtb* were revived in Middlebrooks's 7H9 media supplemented with ADC and subcultured thrice to logarithmic phase (A_{595}, 0.3) by shaking (aerobic). For the hypoxic setup, cultures (from above) were aliquoted in 2-ml cryovials (Sarstedt, Newton, NC) filled to the rim with bacteria, tightly sealed, wrapped with parafilm, and incubated at 37°C for 35 days (hypoxic). The bacteria were lysed, and RNA was purified as described (26).

Survival of *Mtb* and *dos* Mutants

Mtb and mutants were tested for their survival *in vitro* as described (6). The *Mtb* strains were subcultured thrice (A_{595}, 0.4), diluted to A_{595} = 0.1, and grown either with shaking at 220 rpm (aerobic) or standing in tight screw-cap tubes with a headspace ratio of 0.6 (hypoxic). Bacterial CFU counts at defined time points were estimated by plating on 7H10 agar at 37°C. The experiment was performed in triplicate.

Macrophage Infections

Bone marrow–derived macrophages (BMDMs) were isolated from 5- to 6-week-old C3HeB/FeJ mice, stimulated with γ interferon (Gibco; Life Technologies, Grand Island, NY), and infected with *Mtb* H37Rv at an MOI of 1 for 4 hours (7). The cells were washed, and CFU counts were determined.

Host Transcriptomics

After mice were killed, RNA from right lung surgically excised was profiled relative to the RNA from the lung tissue of Day 1 control mice. For macrophage infection studies, RNA was obtained as described (20), and comparisons were performed between cells infected with *Mtb* and Δ-*dos*S. Data were analyzed as described elsewhere

(20, 27–29). Differences in the magnitude of gene expression at Weeks 4, 8, 16, and 20, relative to preinfection, were subjected to statistical analysis using corrected ANOVA. Gene families with significant over-representation were selected for supervised clustering and pathway analyses. Microarray results for a subset of genes were verified by quantitative RT-PCR (primers used are described in Table E1 in the online supplement) as described elsewhere (20). Microarray data, including raw data and images of the present study, have been submitted to Gene Expression Omnibus.

Statistics

Statistical analyses used GraphPad Prism 6.0b (GraphPad Software, La Jolla, CA), Spotfire DecisionSite (Tibco, Boston, MA) for microarray analysis, and ingenuity pathways analysis. Raw and processed microarray data from the experiments included in this article can be accessed from the Gene Expression Omnibus (GEO) using the accession number GSE64645.

Results

Bacterial Burden in C3HeB/FeJ Mice Infected with a Low Dose of *Mtb* and the Various *dos* Mutants

At Day 1, comparable bacillary implantation could be observed for each of the four strains (*Mtb*, *Mtb*:Δ-*dos*R, *Mtb*:Δ-*dos*S, or *Mtb*:Δ-*dos*T) (Figure 1A; Table 1). Hence, there was no defect in the extent of aerosolization or implantation by the different strains.

At Week 4, CFU counts in the lungs of C3HeB/FeJ mice infected with different strains were comparable and averaged between 10^6 and 5×10^6. In *Mtb*-infected animals, the bacterial load increased to approximately 6×10^6 by Week 8 and peaked at 3×10^7 by Week 16 after infection (Figure 1A). In Δ-*dos*R–infected animals, CFU levels were comparable to *Mtb* and peaked at 5×10^7 by Week 20 (Figure 1A). The differences between these groups were not significant. In Δ-*dos*T–infected mice, CFUs were comparable to *Mtb* and Δ-*dos*R initially and were somewhat lower subsequently, although the differences were not statistically significant (Figure 1A). Lung CFUs in mice infected with Δ-*dos*S were, however, about one-half lower relative to *Mtb* at Week 8 and approximately 1.5-logs lower at Week 12. Despite an increase in CFUs at the later stages, Δ-*dos*S bacterial burden remained lower than that of the other strains.

We also studied dissemination of mycobacteria into liver (Figure 1B). Bacilli were detected beginning Week 4. Lower Δ-*dos*S levels were also present in the liver throughout relative to the other strains. Although bacterial burdens for *Mtb*, Δ-*dos*R, and Δ-*dos*T were approximately 10^4 at Weeks 12 and 16, the cognate burden for Δ-*dos*S was 1 to 1.5 log lower; these differences were statistically significant. Attenuation was not observed for Δ-*dos*R or Δ-*dos*T at any time point in the liver (Figure 1B).

Lung CFUs in *Mtb*- and Δ*dos*S-infected mice were validated by diaminobenzidine immunohistochemistry and multilabel confocal microscopy using *Mtb*-specific antibody (18). Although signal was comparable between *Mtb* and Δ-*dos*S at Week 8 (Figure 2A, *upper panel*), considerably less signal was observed for the Δ-*dos*S group at Week 16 (Figure 2A, *lower panel*). At higher magnifications, tubercle bacilli were clearly intracellularly localized (Figures 2A and 2B, *upper panel*). However, at later stages, some of the pathological manifestations in the lungs of infected mice included necrosis-approaching or necrotic lesions. Bacilli from the *Mtb* and the Δ-*dos*S groups appeared to not be associated with any host cells and were therefore extracellular at late stage (Figure 2B, *lower panel*).

Histopathology in C3HeB/FeJ Mice Infected with a Low Dose of *Mtb* and the Various *dos* Mutants

At necropsy, we studied histopathology in the lungs of infected animals. Discrete, widely scattered gross pulmonary lesions became apparent 4 weeks after infection in every group and were best shown at this time point in the Δ-*dos*S group (Figure 3A). At Weeks 8 and 12, lungs from *Mtb*-infected mice contained more extensive lesions than the lesions from the animals infected with Δ-*dos*S (Figure 3). At Week 12, the area occupied by granulomatous lesions in *Mtb*-infected mice was significantly greater relative to mice infected with Δ-*dos*S (Figures 3B and 3C). During Weeks 8 to 16, granulomatous inflammation was comprised primarily of macrophages with aggregates of lymphocytes and with gradual increase in individual foamy macrophages, small aggregates of neutrophils within alveolar spaces, and clusters of cholesterol clefts that became more numerous in all groups

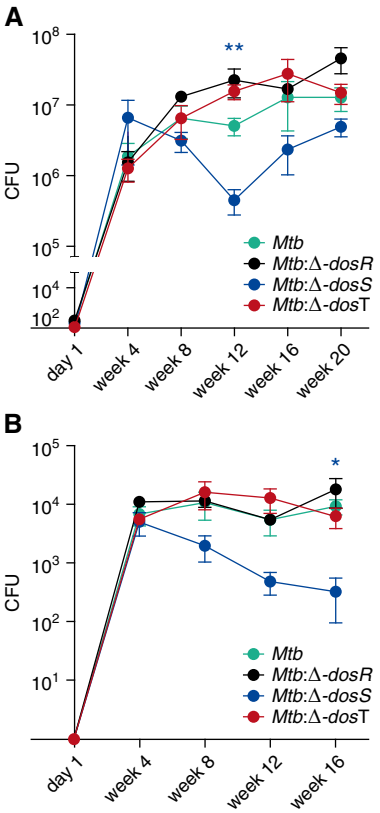

Figure 1. Determination of bacterial burden *in vivo*. Levels of CFUs were determined in the tissues of infected animals at Day 1 and every 4 weeks thereafter. A comparable low-dose infection was established in the lungs of each of the C3HeB/FeJ mice used. *Mtb* (*red*); Δ-*dos*R (*black*); Δ-*dos*S (*blue*); and Δ-*dos*T (*green*). (*A*) CFUs in lungs. (*B*) CFUs in liver. Results are expressed as CFUs in the entire tissue based on weight. $^*P < 0.05$; $^{**}P < 0.005$ (unpaired *t* test). *Mtb*, *Mycobacterium tuberculosis*.

(Figure 4; *see* Figure E1 in the online supplement). One-third of the animals infected with Δ-*dos*S exhibited extensive necrosis within granulomas at Week 20 (Figure 4B) (11, 15).

Immune Response to Infection with the Various Mutants

Global gene expression was used as a measure of immune response in the lungs of C3HeB/FeJ mice infected with *Mtb* and Δ-*dos*S at different time points. Initially, induction of genes involved in the proinflammatory response was observed in both strains. Thus, the expression of chemokine receptors Cxcr3 and Cxcr5, Tnf ligands, and receptor Tnfrsf18 and Ifn-regulated genes Ifi44 and Il1b was induced in *Mtb*- and Δ-*dos*S–infected mice,

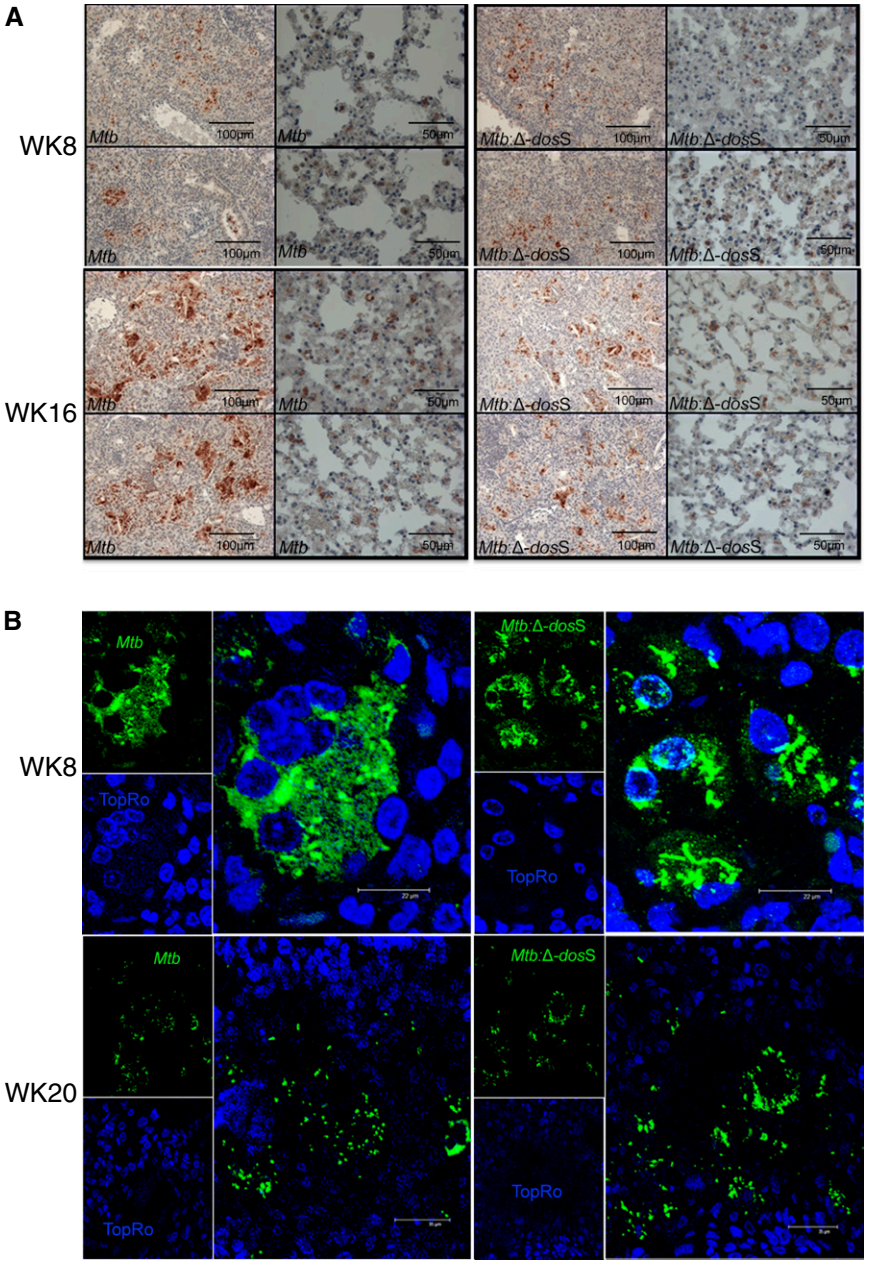

Figure 2. Immunohistochemistry to localize bacilli in the lungs of C3HeB/FeJ mice. (*A*) Diaminobenzidine-based detection of bacilli (*brown color*) in mice lungs infected with *Mtb* or Δ-*dos*S. Two representative images from 10 fields per slide out of a total of three slides per animal are shown. Multiple cells staining positive for bacilli counts are shown on the corresponding higher magnification image to the right of each panel. (*B*) Multilabel confocal microscopy specifically shows the presence of intracellular bacilli (*green signal*) in the lungs of mice infected with *Mtb* (*left*) and the Δ-*dos*S mutant (*right*) or at early time points (e.g., 8 wk after infection) (*top panel*). Lesions with central necrosis were observed for both infection groups at later time points (e.g., Week 20). Here, bacilli were mostly extracellular (*bottom panels*). *Scale bars*: *A*, 100 μm in first and third columns, 50 μm in second and fourth columns; *B*, 22 μm.

respectively, at Week 4. Genes belonging to the categories "Inflammatory response" (Tnfrsf13c, Ltb, Lta, Tnfrsf18, Tnfrsf9, Tnfaip8l1, and Traf4) and "Chemotaxis" (Ccl19 and Cxcr3) were initially (Week 4) overrepresented among genes with significantly increased expression upon infection with Δ-*dos*S, demonstrating successful exposure with this mutant.

The proinflammatory gene expression response was dampened in Δ-*dos*S–infected relative to *Mtb*-infected mice at Week 8 (Figure 5). This was concordant with the CFU and pathology results obtained from the mice infected with Δ-*dos*S (Figures 1–3). The most significant differences at Week 8, the time point at which the decline in Δ-*dos*S levels was first detected, were clustered around TNF receptors and their ligands, type-1 interferon response, and B-cell chemoattractants. Thus, the expression of Cxcl13 (>24-fold) and Ccl19 (~15-fold) was highly induced in the lungs of animals infected with *Mtb*, whereas its expression was induced to significantly lower levels (~5-fold and < 2-fold, respectively) in the lungs of Δ-*dos*S–infected animals at this time point (Figure 5). These two homeostatic chemokines are critical in the formation of granulomas, especially the spatial arrangement of lymphocytes (30), and for the addition of B cells to inducible bronchial associated lymphoid tissue, the presence of which correlates with protection from *Mtb* infection in different models and in humans (31, 32). The expression of several TNF ligands and receptors was induced to significantly high levels in *Mtb*-infected lungs but not in Δ-*dos*S–infected lungs. These included Tnfrsf13b (TACI) and Tnfrsf17, both of which are predominantly expressed by B cells (33) that respond to Cxcl13 stimulus (34); the B cell–activating TNF receptor superfamily member Tnfrsf13c (35); as well as lymphotoxins α and β, which have critical roles in controlling *Mtb* infection (36). The expression of Il1b, which controls *Mtb* infection by promoting TNF activity in macrophages by enhancing the expression of several TNF superfamily ligands and receptors (37), was also strongly induced in the *Mtb*-infected group. By Weeks 16 and 20, the expression of various genes in the categories "Chemokines," "Interleukins," and "Interferons," respectively, was perturbed equally in lungs of mice infected with *Mtb* and Δ-*dos*S (not shown), resulting in the amelioration of the significant differences in expression at these time points. These results are concordant with the increased CFU burdens in C3HeB/FeJ mice in the latter stages of the experiment (Figure 1).

Granulomas Are Hypoxic in the Lungs of C3HeB/FeJ Mouse Infected with *Mtb* and *dos* Mutants

Necrotic TB granulomas have been shown to be hypoxic in human tissues and in

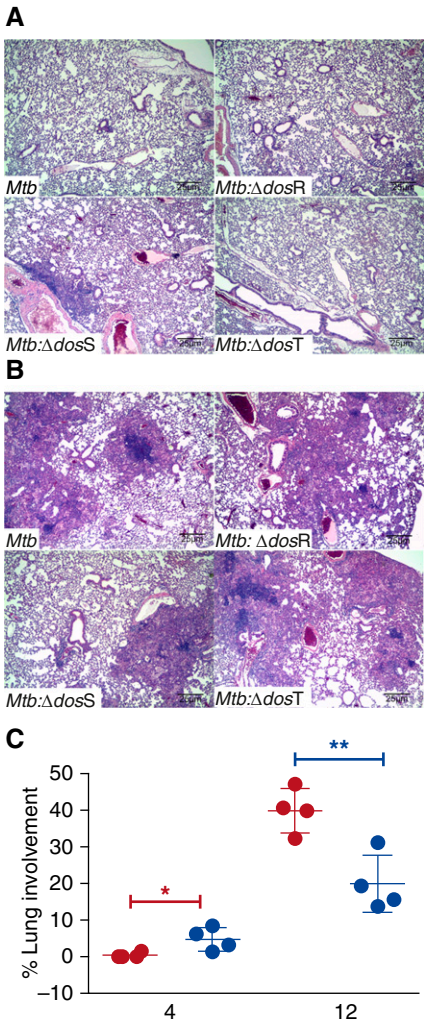

Figure 3. Histopathology analysis. Using hematoxylin and eosin staining, we determined the extent of histopathology in the lungs of animals infected with the different strains over the course of time. (*A*) Day 1. Non-necrotic lung lesions in the early stages of development are composed primarily of lymphocytes and macrophages. (*B*) Week 12. Lesions accumulate neutrophils, foamy macrophages, and numerous cholesterol clefts. (*C*) Percentage of lung area grouped from lung lobes of four mice in *Mtb*- (*red*) and *Mtb*:Δ-*dos*S- (*blue*) infected mice at 4 and 12 weeks after infection. Results show a significant difference at the latter time point. **P* = 0.0330; ***P* = 0.0066 (unpaired *t* test).

various animal models, including nonhuman primates, rabbits, and guinea pigs (38). Such lesions are not observed in the traditional C57Bl/6 mouse model of TB (38). Recently, it was established that lesions in the lungs of *Mtb*-infected C3HeB/FeJ mice become hypoxic (11, 15). We investigated if infection with the Δ-*dos*S strain resulted in the development of such lesions in this mouse strain. The extent of hypoxia in the lungs of C3HeB/FeJ mice infected with *Mtb* and Δ-*dos*S was evaluated at different time points using PIMO adducts (11, 15). Comparable levels of PIMO staining were apparent in the lung lesions of *Mtb*- and Δ-*dos*S–infected animals (Figure 6A). Thus, hypoxia was present in the lung granulomas in C3HeB/FeJ mice, which resulted from infection with Δ-*dos*S. Staining was preferentially observed at the edges of centrally necrotic lesions likely due to the fact that the activation of the product of PIMO requires intact, viable cells. Thus, although hypoxia was clearly present in the lesions originating from either infection, distinct central necrosis was not generally apparent. PIMO staining to a comparable level was also observed in the lung lesions of mice infected with Δ-*dos*R and Δ-*dos*T (not shown).

Effect of Mutations in DosR, DosS, and DosT on the Induction of the DosR Regulon

We investigated the basis of attenuation of Δ-*dos*S observed *in vivo*. Parental *Mtb*, Δ-*dos*R, Δ-*dos*S, and Δ-*dos*T strains were cultured *in vitro*. RNA was isolated from aerobic and hypoxic cultures (6, 39), and transcript levels of *dos*R, *dos*S, *dos*T, and other members of the DosR-regulon (e.g., Rv1738, *hspX*, *tgs1*, etc.) were determined by quantitative RT-PCR. The expression of the entire regulon was adversely affected in the Δ-*dos*R strain during culturing under hypoxia (Figure 6B). However, the expression of *dos*R and *dos*R-dependent genes could be induced to high levels in Δ-*dos*S and Δ-*dos*T strains during hypoxia, despite a clear defect in the induction of the mutated sensor kinase (Figure 6B). For example, the expression of Rv1738, *hspX*, and *tgs1* was induced in hypoxia-treated Δ-*dos*S cultures by more than 100-fold relative to when cultured in aerobic state. In each of these instances, the expression levels were either comparable to or higher than those observed for *Mtb*. Thus, we conclude that Δ-*dos*S and Δ-*dos*T retain the ability to induce the expression of DosR regulon comparable to *Mtb* during hypoxia, likely through the activation of the regulator via another kinase that is functional in absence of one or the other mutation (e.g., DosT in Δ-*dos*S and DosS in Δ-*dos*T mutant). We also assayed the expression levels of *dna*B, which is not regulated by DosR (15), and did not find evidence of its induction in hypoxic *Mtb* cultures.

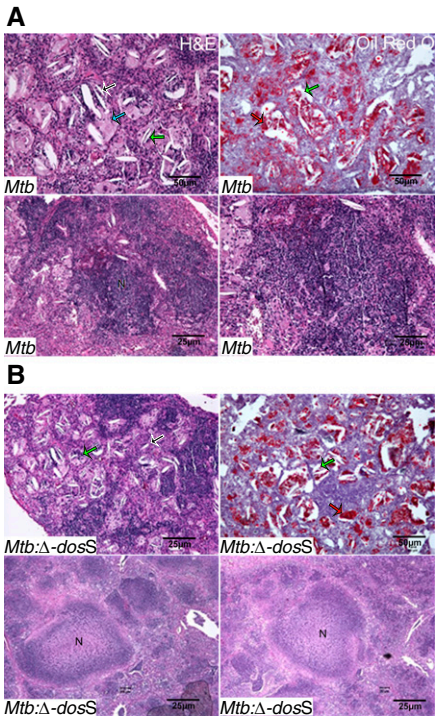

Figure 4. Disease progression in C3HeB/FeJ mice lungs infected with *Mtb* strains. (*A* and *B*, *upper panels*) At Week 16, lesions have individual foamy macrophage (*blue arrow*) with intracellular (*green arrow*) and extracellular (*black arrow*) cholesterol clefts (*upper panel*) stained with Oil Red O, a lipid-staining dye (*red arrow*, *right upper panels* in *A* and *B*) in lungs of mice infected with *Mtb* (*A*) or Δ-*dos*S (*B*). (*A* and *B*, *lower panels*) At Week 20, lesions with necrosis or approaching being nearly necrotic are shown. Stain: hematoxylin and eosin (H&E). N indicates areas of necrosis.

Survival of Δ-*dos*S in Microaerophilic Environment *In Vitro*

Because the mutation in *dos*S did not impede the ability of this strain to induce the DosR regulon, we next analyzed if this mutant exhibited a growth phenotype in an *in vitro* model of microaerophilic growth. The viability of *Mtb*, Δ-*dos*R, Δ-*dos*S, and Δ-*dos*T was assessed for 35 days in aerobic and standing cultures. As shown in Figure 6C, the survival of Δ-*dos*S was not significantly different from that of *Mtb* or for Δ-*dos*R and Δ-*dos*T when cultured in standing conditions *in vitro* for up to 35 days (6). These results indicate that not only does Δ-*dos*S retain the ability to induce the expression of the DosR regulon but that its survival is not compromised during microaerophilic conditions *in vitro* that may mimic hypoxia within human-like granulomas *in vivo*.

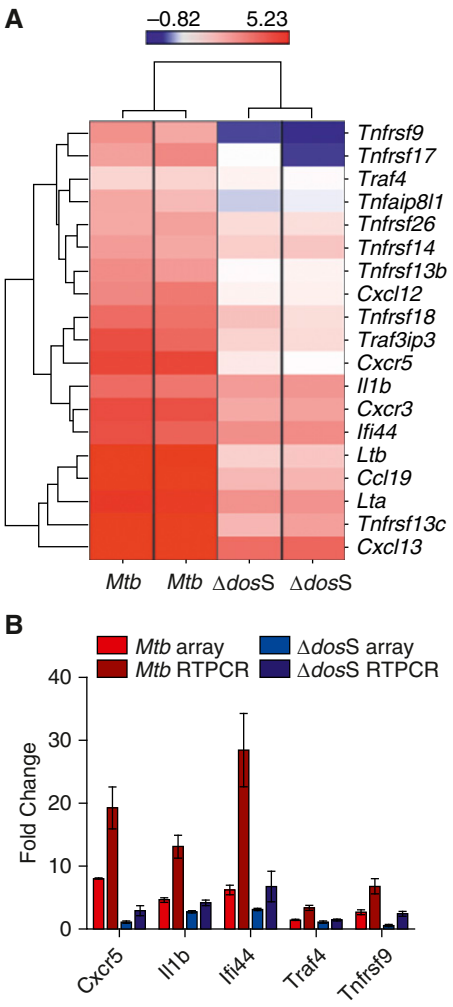

Figure 5. Supervised hierarchical clustering and global gene-ontology analysis. (*A*) Expression of chemokines, interferons/co-regulated genes, and cytokines/TNF c-regulated genes in *Mtb*- and Δ-*dos*S-infected lungs at Week 8. The intensity of *red color* correlates with higher levels of induction; the intensity of *blue color* correlates with higher levels of repression relative to the expression of the same genes in Day 1 (baseline) animals. *Bar* represents the range of gene-expression magnitude. (*B*) The relative fold change in transcripts (*Mtb*-infected mice Week 8 to *Mtb*-infected mice, Day 1) or (Δ-*dos*S-infected mice, Week 8, to Δ-*dos*S-infected mice, Day 1) in microarray (*red* or *blue bars*) and quantitative RT-PCR (*dark red* or *dark blue bars*) is shown.

Comparison of Growth of *Mtb*:Δ-*dos*S with Parental *Mtb* in C3HeB/FeJ Mice–Derived Macrophages *In Vitro*

Having established that the expression of the DosR-regulon was not perturbed in Δ-*dos*S and that this strain did not display a growth defect *in vitro* (as above), we reasoned that the attenuation of Δ-*dos*S *in vivo* was independent of DosR. Previous studies have shown that mutants in *dos*S gene are susceptible to NO donor (40, 41). Because the presence of NO can indicate hypoxia and enhanced phagocyte-derived iNOS response, we assessed if the *in vivo* growth defect observed for Δ-*dos*S in Kramnik mice occurred in cultured macrophages *ex vivo*. Thus, BMDMs isolated from these mice were activated with IFN-γ and infected with *Mtb* and *Mtb*:Δ-*dos*S. Although comparable CFU counts were obtained from the lysates of BMDMs at 0 hours after infection, significantly higher numbers of *Mtb* than Δ-*dos*S bacilli could be recovered after 24 hours of infection (Figure 7A). Thus, the burden of Δ-*dos*S was reduced by 68% at 24 hours, 89% at 72 hours, and 96% at 120 hours relative to *Mtb*. When, as controls, heat-killed *Mtb* (90°C/45 min) were used to infect macrophages, no bacilli were detected at any of the time points.

The host response of BMDMs to infection with *Mtb* and Δ-*dos*S was first compared by quantitative RT-PCR for select macrophage-expressed immune-relevant genes. Cells infected with Δ-*dos*S exhibited higher fold changes of expression for Tnfα, Il1β, Ptgs2, Tnfsf9, and Tnfsf18 at t = 0 hours after infection (as explained in Materials and Methods, the 4-hour infection was succeeded by washing extracellular bacilli, and this time point was considered t = 0). On the other hand, the expression of Mmp9 and S100A8 (32), both correlates of active TB *in vivo*, occurred at a significantly lower level in cells infected with Δ-*dos*S at this time point relative to cells infected with *Mtb* (Figure 7B). These results prompted us to compare in depth the macrophage response to these two strains. Genes with perturbed expression in macrophages infected with Δ-*dos*S mutant compared with *Mtb* are shown in Figure E2. At t = 0 hours, a time point at which bacterial burdens were comparable, in addition to a higher inflammatory response exemplified by induced levels of Tnf, Tnfsf18, Bag4, Creb3l3, Il6, IL1b, and Defa4, the expression of oxidative/nitrosative burst mediators Nos1 (nitric oxide synthase) and Ahr (aryl hydrocarbon receptor) was higher in Δ-*dos*S–infected macrophages relative to the *Mtb*-infected group (Figure E3). This indicates that the reduced burden of Δ-*dos*S *ex vivo* and *in vivo* may be due its inability to resist oxidative/nitrosative stress. Honaker and colleagues have shown that their Δ-*dos*S

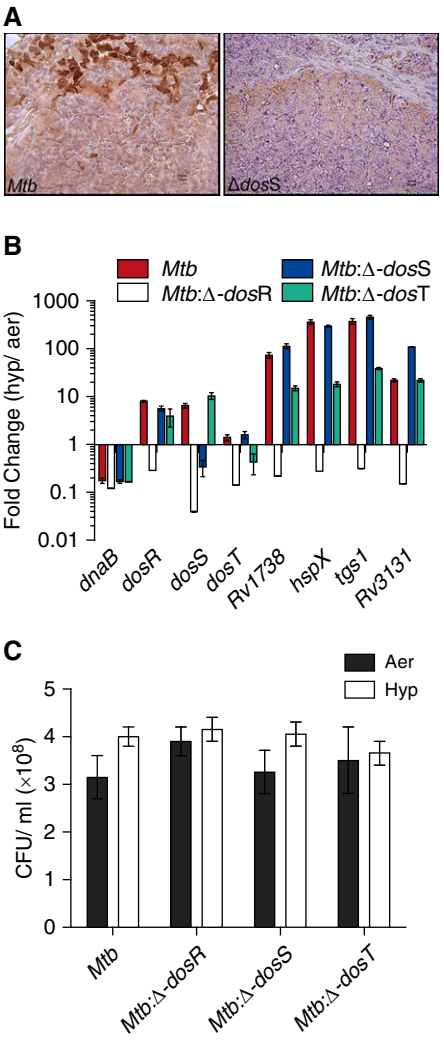

Figure 6. Detection of hypoxia *in vivo* and evaluation of the *in vitro* hypoxia phenotype of the *Mtb*:Δ-*dos*S mutant. (*A*) Immunohistochemistry staining with hypoxia marker pimonidazole in lungs of C3HeB/FeJ mice infected with *Mtb* (*left*) and the *Mtb*:Δ-*dos*S mutant (*right*). Multiple cells stain positive in each of the two images, and the highest intensity is reserved in the inner-ring wall of each of the lesions, where presumably cells are intact, relative to the central necrotic region. (*B*) Quantitative RT-PCR–based evaluation of expression of the various members of the DosR regulon (*dos*R, *dos*S, *dos*T, Rv1738, *hspX, tgs1*, and Rv3131 [39], the various strains grown in hypoxic conditions *in vitro*). *Mtb* (*red*); Δ-*dos*R (*white*); Δ-*dos*S (*blue*); and Δ-*dos*T (*green*). The *y*-axis represents fold change of expression relative to when these strains were cultured in normal aerobic conditions. Results were normalized based on the C_t values for the *Mtb 16S* ribosomal RNA gene as a housekeeping control. (*C*) CFUs per milliliter of *Mtb*, Δ-*dos*R, Δ-*dos*S, and Δ-*dos*T grown in aerobic (Aer) conditions (*solid bar*) and in hypoxic (Hyp) conditions (35-d standing cultures) (*open bar*) are shown. Each *bar* represents results from biological replicate experiments.

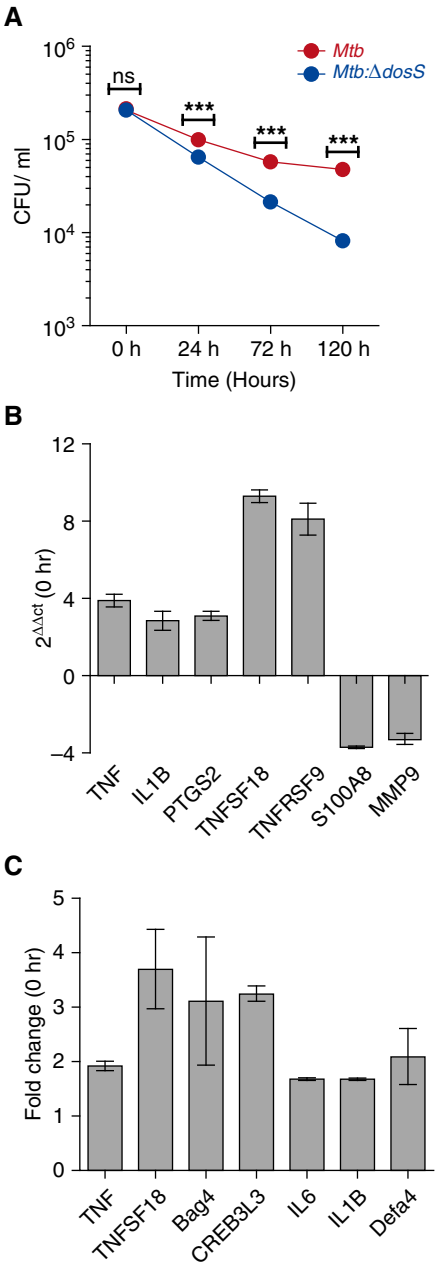

Figure 7. Growth–phenotype comparison of *Mtb*:Δ-*dos*S to *Mtb* C3HeB/FeJ mouse–derived bone marrow–derived macrophages (BMDMs). (*A*) Growth of *Mtb*:Δ-*dos*S was compared with wild-type *Mtb* in IFN-γ–activated C3HeB/FeJ mouse–derived BMDMs. *Mtb* (*red*); Δ-*dos*S (*blue*). Bacterial counts were significantly different at and after 24 hours ($P < 0.0001$; unpaired *t* test). Each *bar* represents results from biological replicate experiments. (*B*) Fold change in regulation of selected genes by quantitative RT-PCR, microarray (*C*) in BMDMs infected with Δ-*dos*S relative *Mtb*. ***$P < 0.005$. ns, not significant.

mutant responds to the stimulus provided by an NO donor via DosR (40). At 24 hours, when Δ-*dos*S CFUs were significantly lower in macrophages relative to *Mtb*, the expression of anti-inflammatory cytokine Il10 was induced, whereas the expression of the proinflammatory signature was repressed.

Discussion

Mtb undoubtedly encounters low oxygen tension during intragranulomatous persistence (42). The DosR regulon has been implicated in the survival of *Mtb* during hypoxia and microaerophilic growth (3, 4, 43, 44). However, the Δ-*dos*R mutant did not exhibit a growth-defect phenotype in C57/Bl6 mice (6). Subsequent studies indicated that Δ-*dos*R exhibits reduced growth in rabbit and guinea pig models (8, 9). A detailed analysis of the role of the entire DosR regulon in pathogenesis has not been performed *in vivo*. We hypothesized that C3HeB/FeJ mice, which develop necrotic-hypoxic TB granulomas (15) and have been used for studying the efficacy of anti-*Mtb* (11) and host-directed (14) drugs, would be ideally suited to study if the DosR regulon is required for both the establishment as well as the maintenance of infection *in vivo*.

Our results show that the virulence of Δ-*dos*R is not altered in C3HeB/FeJ mice relative to *Mtb*. These results are consistent with previous reports where the virulence of Δ-*dos*R was indistinguishable from the parental strain in the C57/Bl6 mouse model (6), where lesions do not develop hypoxia (24). An important result from our study was that DosS appears to be relatively more important than DosT for the *in vivo* virulence and persistence of *Mtb* (Figure 1). Another major finding was that, although infection with Δ-*dos*S resulted in reduced bacterial burden in lungs and liver, fewer lesions, and weakened proinflammatory responses, Δ-*dos*R did not exhibit such a reduction (Figures 1–3). Although the reduced immunopathology noted with Δ-*dos*S infection could be a function of the lower bacterial burden, we exclude the possibility of attenuation due to an intrinsic growth defect because Δ-*dos*S bacilli multiply *in vitro* in a manner comparable to wild-type *Mtb* (Figure 6C). These results suggest that the DosS kinase might regulate hitherto unknown functions independent of DosR. Our results also show that, in addition to chemotherapy studies, this model is valuable for the study of *Mtb* pathogenesis.

These results must be interpreted in the context of findings that lesions from infection with Δ-*dos*S are pathologically indistinguishable from *Mtb* and develop necrosis and hypoxia, especially at later stages (Figures 4 and 6A). In some of the later lesions in both groups, bacilli were present extracellularly (Figure 2B). This conclusively shows that the pathology of the infection with wild-type and the attenuated mutant strain is not different. We conclude that the reduced CFUs and immune responses in mice infected with the mutant are not due its inability to generate necrotic lesions. Support for this contention also comes from the comparable cholesterol clefts and oil red in lesions of both groups (Figure 4) and high-magnification images that show the advent of necrosis in central regions of granulomas as well as strong signal in the periphery after PIMO staining (Figure 6A).

Although it is conceivable that Δ-*dos*S is susceptible to hypoxia, our results outlined in Figures 6B and 6C show that the Δ-*dos*S mutant retains the ability to induce the effector functions of the DosR regulon and is not susceptible to hypoxia in the standing culture model *in vitro*. The expression of *dos*S and *dos*T genes was not found to be induced in Δ-*dos*S and Δ-*dos*T, respectively. However, the expression of the DosR regulon genes (e.g., Rv1738, *hsp*X, and *tgs*1) was induced in both mutants, showing that either *dos*S or *dos*T alone can regulate the DosR regulon. As such, we conclude that the induction of DosR regulon in the Δ-*dos*S mutant is due to the activation of DosR via DosT and *vice versa*. Therefore, we believe that hypoxia in the lung lesions of C3HeB/FeJ mice is not responsible for the partial attenuation of the Δ-*dos*S mutant.

We therefore predicted that the attenuation of Δ-*dos*S mutant results from its inability to withstand stress and studied if its *in vivo* reduced burden phenotype could be replicated in macrophage cultures. Our findings indicate that the reduced bacterial burden of Δ-*dos*S in this study may be due to the inability of these strains to cope with innate antimycobacterial functions mediated by macrophages. Thus,

the expression of Nos1, a constitutive nitric oxide synthase (45), was induced in macrophages infected with Δ-*dos*S relative to those infected with *Mtb*. It is conceivable that Nos1 expression in murine macrophages infected with this mutant can restrict its growth via production of NO, which has antimicrobial functions and which is known to induce the DosR regulon. The differential expression of Ahr (aryl hydrocarbon receptor) and genes in this network was also of interest because it is required for bacterial clearance by promoting macrophage survival and reactive oxygen species production (46).

Our suggestion that DosS may function in a DosR-independent manner may not be without precedent in the biochemistry of *Mtb*, where several regulators are known to interact with molecules other than their primary target or the ones that they were first discovered to interact with. Thus, although the protein encoded by the Rv2745c gene is predicted to induce the expression of Clp protease genes in *Mtb*, it is strongly induced in response to oxidative stress but does not perform its primary function (47). Instead, the function of the ClgR protein under such circumstances is to supplement the high levels of a regulator SigH, which is the primary responder to that stress. Similarly, the 79 toxin–antitoxin pairs encoded by *Mtb* (48), many of which are induced in persister *Mtb* populations, exhibit promiscuous affinities. The *Mtb* MazF9 toxin, for example, is neutralized by the noncognate antitoxins MazE6, VapB27, and VapB40. Thus, it would not be surprising if the DosS sensor kinase activated regulatory proteins in addition to DosR under different circumstances and perhaps at different enzymatic rates. Studies aimed at deciphering these regulatory circuits within the DosR regulon are required. Anecdotal evidence for the fact that the DosR regulon is critical for *Mtb* pathogenesis is provided by its overexpression in strains of the hypervirulent W-Beijing lineage (49). A complete understanding of this process might require studies in the human-like macaque model of TB. ■

Author disclosures are available with the text of this article at www.atsjournals.org.

References

1. Hunter RL, Jagannath C, Actor JK. Pathology of postprimary tuberculosis in humans and mice: contradiction of long-held beliefs. *Tuberculosis (Edinb)* 2007;87:267–278.
2. Russell DG. Who puts the tubercle in tuberculosis? Nature reviews. *Microbiology* 2007;5:39–47.
3. Sherman DR, Voskuil M, Schnappinger D, Liao R, Harrell MI, Schoolnik GK. Regulation of the *Mycobacterium tuberculosis* hypoxic response gene encoding alpha -crystallin. *Proc Natl Acad Sci USA* 2001;98: 7534–7539.
4. Boon C, Dick T. How *Mycobacterium tuberculosis* goes to sleep: the dormancy survival regulator DosR a decade later. *Future Microbiol* 2012;7:513–518.
5. Wayne LG, Sohaskey CD. Nonreplicating persistence of *mycobacterium tuberculosis*. *Annu Rev Microbiol* 2001;55:139–163.
6. Rustad TR, Harrell MI, Liao R, Sherman DR. The enduring hypoxic response of *Mycobacterium tuberculosis*. *PloS One* 2008;3:e1502.
7. Parish T, Smith DA, Kendall S, Casali N, Bancroft GJ, Stoker NG. Deletion of two-component regulatory systems increases the virulence of *Mycobacterium tuberculosis*. *Infect Immun* 2003;71: 1134–1140.
8. Converse PJ, Karakousis PC, Klinkenberg LG, Kesavan AK, Ly LH, Allen SS, Grosset JH, Jain SK, Lamichhane G, Manabe YC, *et al*. Role of the dosR-dosS two-component regulatory system in *Mycobacterium tuberculosis* virulence in three animal models. *Infect Immun* 2009;77: 1230–1237.
9. Malhotra V, Sharma D, Ramanathan VD, Shakila H, Saini DK, Chakravorty S, Das TK, Li Q, Silver RF, Narayanan PR, *et al*. Disruption of response regulator gene, devR, leads to attenuation in virulence of *Mycobacterium tuberculosis*. *FEMS Microbiol Lett* 2004; 231:237–245.
10. Kaufmann SH, Cole ST, Mizrahi V, Rubin E, Nathan C. *Mycobacterium tuberculosis* and the host response. *J Exp Med* 2005;201: 1693–1697.
11. Driver ER, Ryan GJ, Hoff DR, Irwin SM, Basaraba RJ, Kramnik I, Lenaerts AJ, *et al*. Evaluation of a mouse model of necrotic granuloma formation using C3HeB/FeJ mice for testing of drugs against *Mycobacterium tuberculosis*. *Antimicrob Agents Chemother* 2012;56:3181–3195.
12. Kramnik I, Dietrich WF, Demant P, Bloom BR. Genetic control of resistance to experimental infection with virulent *Mycobacterium tuberculosis*. *Proc Natl Acad Sci USA* 2000;97:8560–8565.
13. Pan H, Yan BS, Rojas M, Shebzukhov YV, Zhou H, Kobzik L, Higgins DE, Daly MJ, Bloom BR, Kramnik I, *et al*. Ipr1 gene mediates innate immunity to tuberculosis. *Nature* 2005;434:767–772.
14. Gupta S, Tyagi S, Almeida DV, Maiga MC, Ammerman NC, Bishai WR. Acceleration of tuberculosis treatment by adjunctive therapy with verapamil as an efflux inhibitor. *Am J Respir Crit Care Med* 2013;188: 600–607.
15. Harper J, Skerry C, Davis SL, Tasneen R, Weir M, Kramnik I, Bishai WR, Pomper MG, Nuermberger EL, Jain SK, *et al*. Mouse model of necrotic tuberculosis granulomas develops hypoxic lesions. *J Infect Dis* 2012;205:595–602.
16. Roberts DM, Liao RP, Wisedchaisri G, Hol WG, Sherman DR. Two sensor kinases contribute to the hypoxic response of *Mycobacterium tuberculosis*. *J Biol Chem* 2004;279:23082–23087.
17. Roy CJ, Sivasubramani SK, Dutta NK, Mehra S, Golden NA, Killeen S, Talton JD, Hammoud BE, Didier PJ, Kaushal D, *et al*. Aerosolized gentamicin reduces the burden of tuberculosis in a murine model. *Antimicrob Agents Chemother* 2012;56:883–886.
18. Mehra S, Golden NA, Dutta NK, Midkiff CC, Alvarez X, Doyle LA, Asher M, Russell-Lodrigue K, Monjure C, Roy CJ, *et al*. Reactivation of latent tuberculosis in rhesus macaques by coinfection with simian immunodeficiency virus. *J Med Primatol* 2011;40:233–243.
19. Dutta NK, Mehra S, Didier PJ, Roy CJ, Doyle LA, Alvarez X, Ratterree M, Be NA, Lamichhane G, Jain SK, *et al*. Genetic requirements for the survival of tubercle bacilli in primates. *J Infect Dis* 2010;201: 1743–175.
20. Gautam US, Mehra S, Ahsan MH, Alvarez X, Niu T, Kaushal D. Role of TNF in the altered interaction of dormant *Mycobacterium tuberculosis* with host macrophages. *PLoS One* 2014;9:e95220.
21. Mehra S, Alvarez X, Didier PJ, Doyle LA, Blanchard JL, Lackner AA, Kaushal D, *et al*. Granuloma correlates of protection against tuberculosis and mechanisms of immune modulation by *Mycobacterium tuberculosis*. *J Infect Dis* 2013;207:1115–1127.
22. Mehra S, Golden NA, Stuckey K, Didier PJ, Doyle LA, Russell-Lodrigue KE, Sugimoto C, Hasegawa A, Sivasubramani SK, Roy CJ, Alvarez X, *et al*. The *Mycobacterium tuberculosis* stress response factor SigH is required for bacterial burden as well as immunopathology in primate lungs. *J Infect Dis* 2012;205:1203–1213.
23. Schnappinger D, Ehrt S, Voskuil MI, Liu Y, Mangan JA, Monahan IM, Dolganov G, Efron B, Butcher PD, Nathan C, *et al*. Transcriptional adaptation of *Mycobacterium tuberculosis* within macrophages: insights into the phagosomal environment. *J Exp Med* 2003;198:693–704.
24. Aly S, Wagner K, Keller C, Malm S, Malzan A, Brandau S, Bange FC, Ehlers S, *et al*. Oxygen status of lung granulomas in *Mycobacterium tuberculosis*-infected mice. *J Pathol* 2006;210:298–305.
25. Zhang Y, Goldman S, Baerga R, Zhao Y, Komatsu M, Jin S. Adipose-specific deletion of autophagy-related gene 7 (atg7) in mice reveals a role in adipogenesis. *Proc Natl Acad Sci USA* 2009;106: 19860–19865.

26. Gautam US, Sikri K, Vashist A, Singh V, Tyagi JS. Essentiality of DevR/DosR interaction with SigA for the dormancy survival program in *Mycobacterium tuberculosis*. *J Bacteriol* 2014;196: 790–769.
27. Kaushal D, Naeve CW. Analyzing and visualizing expression data with Spotfire. Curr Protoc Bioinformatics 2004;Chapter 7:Unit 7 9.
28. Liang T, Kimpel MW, McClintick JN, Skillman AR, McCall K, Edenberg HJ, Carr LG, *et al*. Candidate genes for alcohol preference identified by expression profiling in alcohol-preferring and -nonpreferring reciprocal congenic rats. *Genome Biol* 2010;11:R11.
29. Wu JQ, Sasse TR, Saksena MM, Saksena NK. Transcriptome analysis of primary monocytes from HIV-positive patients with differential responses to antiretroviral therapy. *Virol J* 2013;10:361.
30. Khader SA, Rangel-Moreno J, Fountain JJ, Martino CA, Reiley WW, Pearl JE, Winslow GM, Woodland DL, Randall TD, Cooper AM, *et al*. In a murine tuberculosis model, the absence of homeostatic chemokines delays granuloma formation and protective immunity. *J Immunol* 2009;183:8004–8014.
31. Slight SR, Rangel-Moreno J, Gopal R, Lin Y, Fallert Junecko BA, Mehra S, Selman M, Becerril-Villanueva E, Baquera-Heredia J, Pavon L, *et al*. CXCR5(+) T helper cells mediate protective immunity against tuberculosis. *J Clin Invest* 2013;123:712–726.
32. Gopal R, Monin L, Torres D, Slight S, Mehra S, McKenna KC, Fallert Junecko BA, Reinhart TA, Kolls J, Baez-Saldana R, *et al*. S100A8/A9 proteins mediate neutrophilic inflammation and lung pathology during tuberculosis. *Am J Respir Crit Care Med* 2013;188: 1137–1146.
33. Uslu K, Coleman AS, Allman WR, Katsenelson N, Bram RJ, Alugupalli KR, Akkoyunlu M, *et al*. Impaired B cell receptor signaling is responsible for reduced TACI expression and function in X–linked immunodeficient mice. *J Immunol* 2014;192:3582–3595.
34. Legler DF, Loetscher M, Roos RS, Clark-Lewis I, Baggiolini M, Moser B. B cell-attracting chemokine 1, a human CXC chemokine expressed in lymphoid tissues, selectively attracts B lymphocytes via BLR1/ CXCR5. *J Exp Med* 1998;187:655–660.
35. Thompson JS, Bixler SA, Qian F, Vora K, Scott ML, Cachero TG, Hession C, Schneider P, Sizing ID, Mullen C, *et al*. BAFF-R, a newly identified TNF receptor that specifically interacts with BAFF. *Science* 2001;293:2108–2111.
36. Ehlers S, Holscher C, Scheu S, Tertilt C, Hehlgans T, Suwinski J, Endres R, Pfeffer K, *et al*. The lymphotoxin beta receptor is critically involved in controlling infections with the intracellular pathogens *Mycobacterium tuberculosis* and *Listeria monocytogenes*. *J Immunol* 2003;170:5210–5218.
37. Jayaraman P, Sada-Ovalle I, Nishimura T, Anderson AC, Kuchroo VK, Remold HG, Behar SM, *et al*. IL-1beta promotes antimicrobial immunity in macrophages by regulating TNFR signaling and caspase-3 activation. *J Immunol* 2013;190:4196–4204.
38. Via LE, Lin PL, Ray SM, Carrillo J, Allen SS, Eum SY, Taylor K, Klein E, Manjunatha U, Gonzales J, *et al*. Tuberculous granulomas are hypoxic in guinea pigs, rabbits, and nonhuman primates. *Infect Immun* 2008;76:2333–2340.
39. Gautam US, Sikri K, Tyagi JS. The residue threonine 82 of DevR (DosR) is essential for DevR activation and function in *Mycobacterium tuberculosis* despite its atypical location. *J Bacteriol* 2011;193:4849–4858.
40. Honaker RW, Leistikow RL, Bartek IL, Voskuil MI. Unique roles of DosT and DosS in DosR regulon induction and *Mycobacterium tuberculosis* dormancy. *Infect Immun* 2009;77:3258–3263.
41. Taneja NK, Dhingra S, Mittal A, Naresh M, Tyagi JS. *Mycobacterium tuberculosis* transcriptional adaptation, growth arrest and dormancy phenotype development is triggered by vitamin C. *PLoS One* 2010;5: e10860.
42. Wayne LG, Diaz GA. Autolysis and secondary growth of *Mycobacterium tuberculosis* in submerged culture. *J Bacteriol* 1967;93:1374–1381.
43. Park HD, Guinn KM, Harrell MI, Liao R, Voskuil MI, Tompa M, Schoolnik GK, Sherman DR, *et al*. Rv3133c/dosR is a transcription factor that mediates the hypoxic response of *Mycobacterium tuberculosis*. *Mol Microbiol* 2003;48:833–843.
44. Voskuil MI, Schnappinger D, Visconti KC, Harrell MI, Dolganov GM, Sherman DR, Schoolnik GK, *et al*. Inhibition of respiration by nitric oxide induces a *Mycobacterium tuberculosis* dormancy program. *J Exp Med* 2003;198:705–713.
45. Cunningham-Bussel A, Zhang T, Nathan CF. Nitrite produced by *Mycobacterium tuberculosis* in human macrophages in physiologic oxygen impacts bacterial ATP consumption and gene expression. *Proc Natl Acad Sci USA* 2013;110):E4256–E4265.
46. Kimura A, Abe H, Tsuruta S, Chiba S, Fujii-Kuriyama Y, Sekiya T, Morita R, Yoshimura A, *et al*. Aryl hydrocarbon receptor protects against bacterial infection by promoting macrophage survival and reactive oxygen species production. *Int Immunol* 2014;26:209–220.
47. McGillivray A, Golden NA, Gautam US, Mehra S, Kaushal D. The *Mycobacterium tuberculosis* Rv2745c plays an important role in responding to redox Stress. *PLoS One* 2014;9:e93604.
48. Sala A, Bordes P, Genevaux P. Multiple toxin-antitoxin systems in *Mycobacterium tuberculosis*. *Toxins.* 2014;6:1002–1020.
49. Reed MB, Gagneux S, Deriemer K, Small PM, Barry CE III. The W-Beijing lineage of *Mycobacterium tuberculosis* overproduces triglycerides and has the DosR dormancy regulon constitutively upregulated. *J Bacteriol* 2007;189:2583–2589.